CHINESE OPTICS LETTERS

Vol. 19, No. 3 | March 2021

# Tunable phase-shifted fiber Bragg grating based on a microchannel fabricated by a femtosecond laser

Li Zeng (曾 理), Xiaoyan Sun (孙小燕)*, Zikun Chang (苌子坤), Youwang Hu (胡友旺), and Ji'an Duan (段吉安)

State Key Laboratory of High Performance Complex Manufacturing, College of Mechanical and Electrical Engineering, Central South University, Changsha 410083, China

*Corresponding author: sunxy@csu.edu.cn

Received November 29, 2020 | Accepted January 19, 2021 | Posted Online March 10, 2021

A phase-shifted fiber Bragg grating (PS-FBG) based on a microchannel was proposed and realized by combining the point-by-point scanning method with chemical etching. The PS-FBG is composed of a fiber Bragg grating (FBG) and a microchannel through the fiber core. The microchannel can introduce phase shift into the FBG. What is more important is that it exposes the fiber core to the external environment. The phase shift peak is sensitive to the liquid refractive index, and it shows a linear refractive index response wavelength and intensity sensitivity of 2.526 nm/RIU and −111 dB/RIU, respectively. Therefore, such gratings can be used as sensors or tunable filters.

**Keywords:** fiber Bragg grating; microchannel structure; phase shift; fiber optic sensors.
**DOI:** 10.3788/COL202119.030602

## 1. Introduction

Fiber Bragg gratings (FBGs) have the advantages of small volume, small transmission loss, anti-electromagnetic interference, etc. They are widely used in the field of optical communication and optical fiber sensors[1–7]. Phase-shifted FBGs (PS-FBGs) open one or more narrow band transmission windows in the Bragg reflection spectrum. Therefore, the PS-FBG not only has the advantages of FBGs but also is one type of the most successful band-pass filter due to its unique spectral characteristics; therefore, it has a wide range of applications in dense wavelength division multiplexing (DWDM), tunable narrow band filters, and distributed feedback fiber lasers[8–14]. In addition, different phase shift introduction methods will bring unique sensing characteristics to the PS-FBGs, such as refractive index (RI)[15], magnetic field[16], gas pressure[17], and light polarization[18]. The ultra-narrow transmission peak has a higher accuracy for sensing detection.

The phase-mask technique that employs a phase-shifted phase mask in the single exposure process is one of the most widely used techniques to fabricate PS-FBGs[19]. Although this method is efficient and repeatable, it has poor flexibility. In previous studies, there are many techniques to fabricate PS-FBGs. It can be divided into two categories according to the phase shift introduction mode. One is inducing phase shift during the FBG inscription process. The phase shifts can be induced during the femtosecond (fs) laser direct point-by-point inscription process with a piezoelectric actuator[20], which rapidly shifts the fiber along the direction of its movement in a chosen point of the grating with a chosen shift value. Using an electro-optic amplitude modulator can generate a defined delay between two identical laser pulse trains during the point-by-point inscription process, which offers a high grade of flexibility for grating parameters[21]. Using a variable-velocity scanning UV laser beam in combination with a shielded phase mask can also fabricate PS-FBGs[22]. This kind of method can control the phase shift accurately and flexibly, but it needs additional apparatus, and its cost is high. The other category is to use the post-processing technique to induce phase shift in FBGs. A central region of grating is irradiated by an fs laser assisted with a rotating jig, which produces a $\pi$ phase shift at the central region of the grating and forms a $\pi$ PS-FBG[23]. A PS-FBG can also be formed by two FBG sections with a micrometer-level gap between them that is filled with microfluidic magnetic fluid[16] or photosensitive adhesive[24]. Another PS-FBG can be fabricated by combining fs laser micromachining with fusion splicing. The post-processing technique does not need complex optical devices. However, phase shift is not as accurate as the former category. In addition, there is a quite new technique used recently with fs lasers to inscribe PS-FBGs. This technique is based on inscribing two gratings on the same spot with a wavelength shift. This can be done by strain[25] or tilt[26]. This method is simple and efficient, but the sensing characteristics of the phase shift peak are the same as FBGs. In addition, fs laser-induced selective chemical etching technology can be used to fabricate microstructures in silica fiber, such as microchannel[27] and micro-grooves[28]. These microstructures can enhance the performance of optical fiber sensors[29].

© 2021 Chinese Optics Letters

In this paper, we proposed a new technique to fabricate tunable PS-FBGs, which combined fs laser processing and chemical etching. An FBG is fabricated in a fiber core by the fs laser point-by-point technique, using an fs laser to scribe a line through the fiber in the middle of grating. Finally, the fiber is immersed in the hydrofluoric acid (HF) solution to etch a microchannel. The sensing characteristics of the device to the liquid RI and temperature have been experimentally investigated. With the increase of the liquid RI, the magnitude of the phase-shift experiences a linear decline, and the central wavelength experiences a linear red shift. With the increase of temperature, the reflection spectrum of the device experiences a red shift linearly, while the phase-shift value is hardly changed.

## 2. Fabrication of PS-FBG

Our fabrication system is based on the fs laser point-by-point technique. The experimental setup is shown in Fig. 1. The fs laser system emits laser pulses with a central wavelength of 800 nm and a pulse duration of 120 fs at a repetition of 1 kHz. The pulse energy is attenuated by a half-wave plate and a Glan–Taylor prism to 0.6 μJ. The laser beam is focused in the fiber core by a 100× immersion microscope objective, and the fiber is immersed in oil with an RI of 1.52 to minimize the secondary focusing effect and moved by a high precision electric displacement platform. The monitoring system consists of a spectrometer, a light source, and a 3 dB coupler. The spectral growth is monitored in real time during processing.

The schematic diagram of the designed PS-FBG is shown in Fig. 2, in which a microchannel is positioned in the center of the FBG. The microchannel can introduce a phase shift into the FBG. The fabrication procedure involved three steps. First, a 3 mm long FBG with a period of 1.071 μm was written in the single-mode fiber (SMF-28) with the fs laser point-by-point technique. Then, 0.6 mW fs laser pulses with the repetition rate of 1 kHz are used to inscribe a trace through the middle of the Bragg grating at a speed of 40 μm/s. After the second step, we can obtain the device that is shown in Fig. 3(a), and the spectrum of FBG did not change. However, the trace damaged by the fs laser is more easily corroded by HF. Third, the modified FBG is

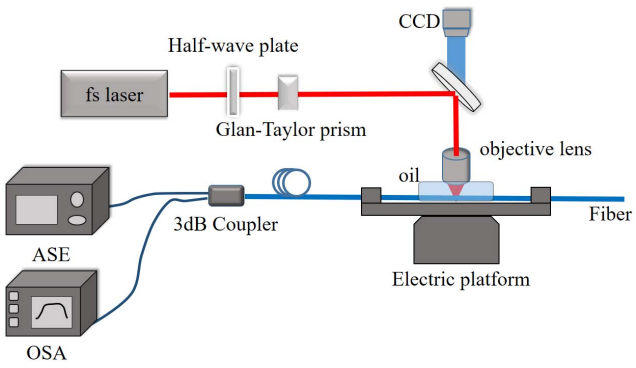


**Fig. 1.** Schematic diagram of the PS-FBG inscription process.

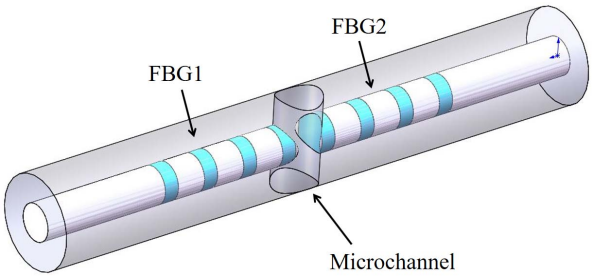


**Fig. 2.** Schematic diagram of the designed PS-FBG.

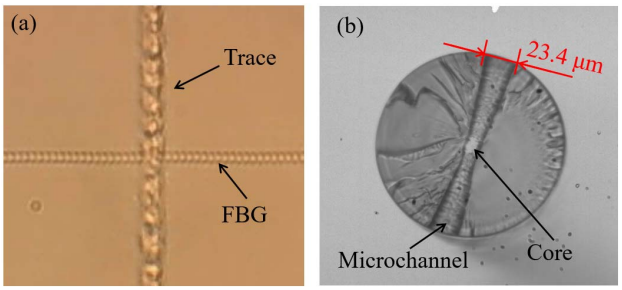


**Fig. 3.** (a) FBG and trace image observed in CCD and (b) optical microscope image of the fiber end face.

immersed into 5% HF solution for corrosion. At the same time, an ultrasound with the frequency of 20 kHz is used to assist the corrosion. An ultrasound can reduce the corrosion time, thereby reducing the diameter of the microchannel and increasing the device strength. During the corrosion process, the spectrum is monitored by an optical spectrum analyzer (OSA). In order to check the microchannel, a fabricated device is cleaved at the microchannel. The optical microscope image of the fiber end face is shown in Fig. 3(b). A microchannel is successfully fabricated through the fiber. The original FBG is divided into FBG1 and FBG2. The microchannel allows the external liquid to flow through the fiber, making the phase shift peak more sensitive to the RI of the external liquid.

The spectrum of the PS-FBG during the etching process is shown in Fig. 4. It remains unchanged during the first 14 min of corrosion because the HF has not yet corroded the fiber core. The central wavelength of the FBG is 1549.68 nm, and the 3 dB bandwidth is 364 pm. In this device, phase shift is induced by the microchannel; therefore, the phase shift depends on the diameter of the microchannel. It can be seen from Fig. 4, as HF enters the fiber core, the phase shift peak appears. As the etching progresses, the phase shift peak continues to shift. Therefore, the phase shift peaks with different central wavelengths can be obtained by controlling corrosion time. When the central wavelength of the phase shift peak approaches the peak of the original Bragg grating, the intensity of the phase shift peak reaches the maximum. As is shown in the Fig. 4(d), when the central wavelength reaches 1549.79 nm, the intensity of the phase shift peak reaches 8.14 dB. The 3 dB bandwidth of the phase shift peak is 96 pm, which is only a quarter of the FBG.

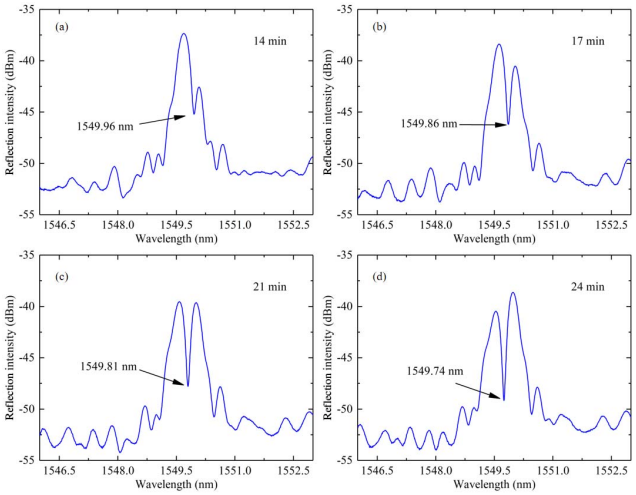


**Fig. 4.** Spectrum of the PS-FBG at different times during the corrosion process: (a) 14 min, (b) 17 min, (c) 21 min, and (d) 24 min.

## 3. Refractive Index and Temperature Sensitivity

We put the device into different concentrations of glycerol solution to investigate the influence of the RI on the phase shift peaks. The experimental result is shown in Fig. 5. When the RI gradually increased from 1.364 to 1.413, the phase shift peak experienced a red shift. At the same time, the intensity of the phase shift peak also decreased. The phase shift is induced by the microchannel that passes the light in the fiber through the external liquid. Even if the RI of liquid changes slightly, the phase shift peak will change obviously. The phase-shifted value $\varphi$ in our experiment can be derived from[17,30]

$$\varphi = \frac{2\pi n_l D}{\lambda} + \frac{n_0 \tanh(\pi n_1 L_1/\lambda)}{n_1} + \frac{n_0 \tanh(\pi n_2 L_2/\lambda)}{n_2}, \quad (1)$$

where $n_l$ is the RI of the liquid in the microchannel, $n_1$, $n_2$, and $n_0$ are the $n_{\text{eff}}$ of FBG1, FBG2, and the fiber core, respectively. The phase shift depends on the liquid RI in the microchannel and the lengths of FBG1 ($L_1$), FBG2 ($L_2$), and the diameter ($D$) of the microchannel. According to Eq. (1), the relationship between the phase shift $\Delta\varphi$ and changes in the RI of external liquid $\Delta n_l$ can be expressed as

$$\Delta\varphi = \frac{2\pi D}{\lambda}\Delta n_l. \quad (2)$$

From Eq. (2), phase shifts gradually accumulate as the RI increases. It is consistent with the experimental results that the phase shifts experience a red shift.

We extracted the wavelength and intensity of the phase shift peak in different RI liquids and made a linear fitting; the results are shown in the Fig. 6. The sensitivity is 2.526 nm/RIU and −111 dB/RIU, respectively. Compared with the sensitivity of the central wavelength, the sensitivity of the intensity to the change of the RI is high. Therefore, our device can be used as a highly sensitive intensity modulated liquid RI sensor.

We immerse the PS-FBG in distilled water and gradually increase the water temperature from 23.5°C to 79.7°C to investigate the influence of temperature on the PS-FBG. The reflection spectrum at different temperatures is shown in Fig. 7. There are three extreme points in each PS-FBG reflection spectrum, which were phase shift peak, $R_1$, and $R_2$, respectively. When the temperature increases, the three extreme points are red-shifted synchronously. It indicates that the increase of temperature can hardly change the introduced phase shift. The RI of the distilled water and fiber core changes very little when the temperature gradually increases from 23.5°C to 79.7°C. According to Eq. (1), the phase shift also changes slightly. Thus, the three extreme points are red-shifted synchronously.

The linear relationship between the wavelength and temperature of the three extreme points is shown in Fig. 8. The temperature sensitivities of the phase shift peak, $R_1$, and $R_2$ are 9.66 pm/°C, 9.64 pm/°C, and 9.86 pm/°C, respectively, which are similar to the FBG. According to the coupled mode theory, $\lambda_B$ satisfies the relation of Eq. (3):

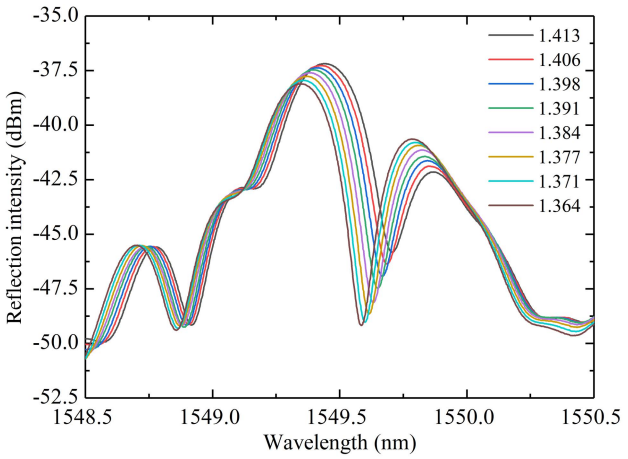


**Fig. 5.** Reflection spectra varying with the refractive index.

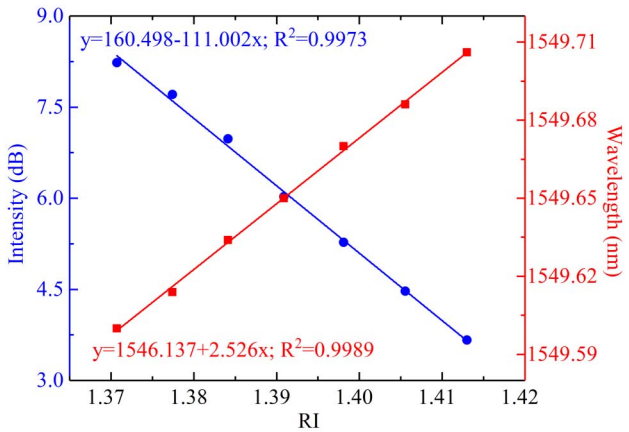


**Fig. 6.** Linear relationship between the wavelength and refractive index of the phase shift peak (red line). Linear relationship between the intensity and refractive index of the phase shift peak (blue line).

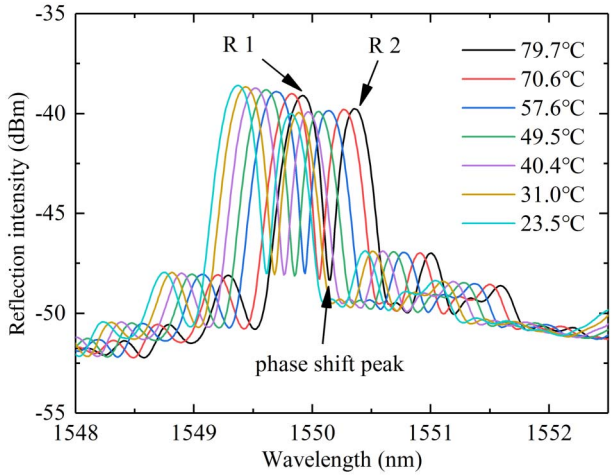


**Fig. 7.** Reflection spectra of the microchannel PS-FBG in distilled water at different temperatures.

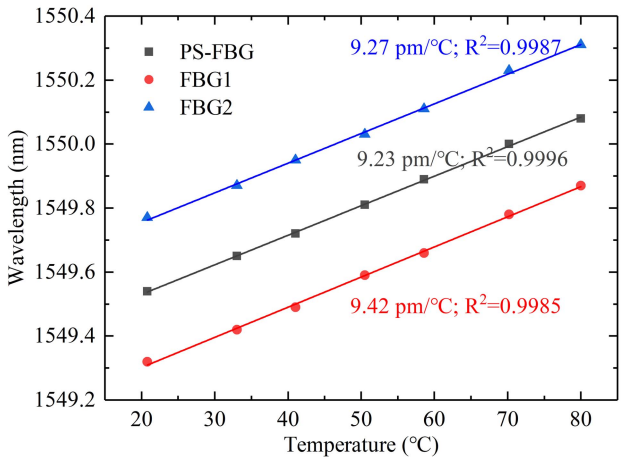


**Fig. 8.** Linear relationship between the wavelength and temperature of the three extreme points.

$$\lambda_B = 2n_{\text{eff}}\Lambda. \tag{3}$$

When the temperature changes, it will cause changes in $n_{\text{eff}}$ and $\Lambda$. Therefore, the FBG wavelength shift caused by the temperature is expressed as Eq. (4):

$$\Delta\lambda_B = 2(\Delta n_{\text{eff}}\Lambda + n_{\text{eff}}\Delta\Lambda). \tag{4}$$

The thermo-optic effect makes the $n_{\text{eff}}$ change, and the thermal expansion of the fiber makes $\Lambda$ change. Thus, Eq. (4) can be converted to Eq. (5):

$$\frac{\Delta\lambda}{\lambda} = (\alpha + \xi)\Delta T. \tag{5}$$

For the fused silica fiber coefficient of thermal expansion $\alpha = 5.5\times10^{-7}\,^{\circ}\text{C}^{-1}$ and thermo-optic coefficient $\xi = 7\times10^{-6}\,^{\circ}\text{C}^{-1}$, $\alpha$ is one order of magnitude smaller than $\xi$. Therefore, the effect of thermal expansion on $\lambda_B$ is negligible. Thus, the increase of temperature will cause the spectrum to shift to the long-wavelength direction, but it has little effect on the phase shift that is introduced by the microchannel. When $\lambda_B$ is 1550 nm, the theoretical sensitivity is 11.7 pm/°C, which is consistent with our experimental results.

## 4. Summary

In summary, we have experimentally demonstrated a novel method to fabricate tunable PS-FBGs by combining fs laser processing together with chemical etching. First, we use the fs laser point-by-point technique to inscribe an FBG in the fiber core. Then, a line through the fiber in the middle of the grating is inscribed with the fs laser. Finally, the fiber is immersed in HF to corrode a microchannel. Different central wavelengths of phase shift peaks can be obtained by controlling the corrosion time. Besides, the central wavelength and intensity of the phase shift peak can also be tuned by the increase of the surrounding RI with sensitivity of 2.526 nm/RIU and −111 dB/RIU, respectively. When the temperature increases, there is no additional phase shift. The spectrum experiences a red shift, and the three extreme points have similar temperature sensitivities. Therefore, this type of PS-FBG can be used in optical communication and optical fiber sensing. Besides, filling the microchannel with special liquid can make it have special applications in the petrochemical industry or biomedicine.

## Acknowledgement

This work was supported by the National Natural Science Foundation of China (Nos. 51875584, 51935013, and 51875585) and the National Key R&D Program of China (Nos. 2018YFB1107803 and 2017YFB1104800).

## References

1. S. Gao, M. Luo, Z. Jing, and H. Chen, "A tunable dual-wavelength fiber ring-cavity laser based on a FBG and DFB laser injection," Optik **203**, 163961 (2020).
2. C. Li, C. Liao, J. Wang, Z. Li, Y. Wang, J. He, Z. Bai, and Y. Wang, "Femtosecond laser microprinting of a polymer fiber Bragg grating for high-sensitivity temperature measurements," Opt. Lett. **43**, 3409 (2018).
3. Y. Ma, X. Qiao, T. Guo, R. Wang, J. Zhang, Y. Weng, Q. Rong, M. Hu, and Z. Feng, "Reflective fiber-optic refractometer based on a thin-core fiber tailored Bragg grating reflection," Opt. Lett. **37**, 323 (2012).
4. L. Yinggang, L. Xin, Z. Ting, and Z. Wei, "Integrated FPI-FBG composite all-fiber sensor for simultaneous measurement of liquid refractive index and temperature," Opt. Laser Eng. **111**, 167 (2018).
5. L. Zhang, F. Yan, T. Feng, W. Han, Y. Bai, Z. Bai, D. Cheng, H. Zhou, and Y. Suo, "Wavelength-tunable thulium-doped fiber laser with sampled fiber Bragg gratings," Opt. Laser Technol. **120**, 105707 (2019).
6. H. Li, Q. Zhao, S. Jiang, J. Ni, and C. Wang, "FP cavity and FBG cascaded optical fiber temperature and pressure sensor," Chin. Opt. Lett. **17**, 040603 (2019).
7. X. Fan, J. Jiang, X. Zhang, K. Liu, S. Wang, and T. Liu, "Investigation on temperature characteristics of weak fiber Bragg gratings in a wide range," Chin. Opt. Lett. **17**, 120603 (2019).

8. E. Xu, S. Pan, Z. Zhang, and P. Li, "Performance-improved microwave photonic single-passband filter using birefringence of phase-shifted fiber Bragg grating," Opt. Commun. **428**, 41 (2018).
9. Z. Glasser, Y. Ofer, R. Abramov, D. Gotliv, and S. Sternklar, "High speed and high sensitivity fiber Bragg grating interrogator based on the RF phase-shift technique," Opt. Commun. **428**, 240 (2018).
10. A. Zhang, L. Hao, B. Geng, and D. Li, "Investigation of narrow band random fiber ring laser based on random phase-shift Bragg grating," Opt. Laser Technol. **116**, 1 (2019).
11. X. Zhao, M. Dong, Y. Zhang, H. Niu, F. Luo, and L. Zhu, "Switchable dual-wavelength fiber laser based on a phase-shifted fiber Bragg grating combined with Mach–Zehnder interferometer and Sagnac loop," Opt. Fiber Technol. **48**, 104 (2019).
12. C. Sun, M. Wang, Y. Dong, S. Ye, and S. Jian, "Compound comb filter based on Sagnac interferometer and phase shifted fiber Bragg grating using for tunable and switchable fiber ring laser," Laser Phys. **28**, 105102 (2018).
13. Y. Ma, Z. Zhang, J. Yuan, Z. Zeng, S. Zhang, Y. Zhang, Z. Zhang, D. Fu, J. Wang, and Y. Liu, "Optically tunable microwave frequency downconversion based on an optoelectronic oscillator employing a phase-shifted fiber Bragg grating," IEEE Photon. J. **10**, 5501611 (2018).
14. S. Miao, W. Zhang, and Y. Song, "Random Bragg-gratings-based narrow linewidth random fiber laser with a π-phase-shifted FBG," Chin. Opt. Lett. **17**, 071403 (2019).
15. C. Liao, L. Xu, C. Wang, D. N. Wang, Y. Wang, Q. Wang, K. Yang, Z. Li, X. Zhong, J. Zhou, and Y. Liu, "Tunable phase-shifted fiber Bragg grating based on femtosecond laser fabricated in-grating bubble," Opt. Lett. **38**, 4473 (2013).
16. L. Bao, X. Dong, S. Zhang, C. Shen, and P. P. Shum, "Magnetic field sensor based on magnetic fluid-infiltrated phase-shifted fiber Bragg grating," IEEE Sens. J. **18**, 4008 (2018).
17. J. Luo, S. Liu, Y. Zhao, Y. Chen, K. Yang, K. Guo, J. He, C. Liao, and Y. Wang, "Phase-shifted fiber Bragg grating modulated by a hollow cavity for measuring gas pressure," Opt. Lett. **45**, 507 (2020).
18. A. Halstuch and A. A. Ishaaya, "Characterizing the effect of femtosecond photo-treatment on the center wavelength of fiber Bragg gratings," Opt. Express **26**, 18990 (2018).
19. C. Martinez and P. Ferdinand, "Analysis of phase-shifted fiber Bragg gratings written with phase plates," Appl. Opt. **38**, 3223 (1999).
20. X. Chen, Y. Painchaud, K. Ogusu, and H. Li, "Phase shifts induced by the piezoelectric transducers attached to a linearly chirped fiber Bragg grating," J. Lightwave Technol. **28**, 2017 (2010).
21. J. Burgmeier, C. Waltermann, G. Flachenecker, and W. Schade, "Point-by-point inscription of phase-shifted fiber Bragg gratings with electro-optic amplitude modulated femtosecond laser pulses," Opt. Lett. **39**, 540 (2014).
22. J. Zhou, K. Guo, J. He, M. Hou, Z. Zhang, C. Liao, Y. Wang, G. Xu, and Y. Wang, "Novel fabrication technique for phase-shifted fiber Bragg gratings using a variable-velocity scanning beam and a shielded phase mask," Opt. Express **26**, 13311 (2018).
23. X. Zhou, Y. Dai, J. M. Karanja, F. Liu, and M. Yang, "Fabricating phase-shifted fiber Bragg grating by simple postprocessing using femtosecond laser," Opt. Eng. **56**, 27108 (2017).
24. D. Yang, Y. Liu, Y. Wang, T. Zhang, M. Shao, D. Yu, H. Fu, and Z. Jia, "Integrated optic-fiber sensor based on enclosed EFPI and structural phase-shift for discriminating measurement of temperature, pressure and RI," Opt. Laser Technol. **126**, 106112 (2020).
25. A. Halstuch and A. A. Ishaaya, "Strain-assisted femtosecond inscription of phase-shifted gratings," Opt. Lett. **43**, 3893 (2018).
26. X. Sun, L. Zeng, H. Du, X. Dong, Z. Chang, Y. Hu, and J. Duan, "Phase-shifted gratings fabricated with femtosecond laser by overlapped two types of fiber Bragg gratings," Opt. Laser Technol. **124**, 105969 (2020).
27. D. Chu, X. Sun, Y. Hu, X. Dong, and K. Yin, "Micro-channel etching characteristics enhancement by femtosecond laser processing high-temperature lattice in fused silica glass," Chin. Opt. Lett. **15**, 071403 (2017).
28. W. He, Y. Fang, L. Zhu, M. Dong, X. Lou, and F. Luo, "Optical fiber interference sensor based on fiber ending micro-groove fabricated by femtosecond laser," Optik **158**, 1295 (2018).
29. S. Schulze, M. Wehrhold, and C. Hille, "Femtosecond-pulsed laser written and etched fiber Bragg gratings for fiber-optical biosensing," Sensors **18**, 2844 (2018).
30. Y. O. Barmenkov, D. Zalvidea, S. Torres-Peiró, J. L. Cruz, and M. V. Andrés, "Effective length of short Fabry–Perot cavity formed by uniform fiber Bragg gratings," Opt. Express **14**, 6394 (2006).